5-17-2012

Azimuthal Dependence of Switching Field Strength for Nematic Liquid Crystal Bistability on Patterned Alignment Layers

Jun-ichi Niitsuma

Makoto Yoneya

Hiroshi Yokoyama
Kent State University - Kent Campus, hyokoyam@kent.edu

Azimuthal dependence of switching field strength for nematic liquid crystal bistability on patterned alignment layers

Jun-ichi Niitsuma,[1,2,a)] Makoto Yoneya,[1,3] and Hiroshi Yokoyama[1,4]
[1]*Liquid Crystal Nano-System Project, ERATO/SORST, Japan Science and Technology Agency, 5-9-9 Tokodai, Tsukuba 300-2635, Japan*
[2]*School of Materials Science, Japan Advanced Institute of Science and Technology, 1-1 Asahidai, Nomi, Ishikawa 923-1292, Japan*
[3]*Nanosystem Research Institute, National Institute of Advanced Industrial Science and Technology (AIST), 1-1-1 Umezono, Tsukuba 305-8568, Japan*
[4]*Liquid Crystal Institute, Kent State University, P.O. Box 5190, Kent, Ohio 44242-0001, USA*

(Received 12 January 2012; accepted 14 April 2012; published online 17 May 2012)

We investigate the azimuthal dependence of the switching field strength for nematic liquid crystal bistability on patterned alignment layers to determine the validity of a switching theory proposed by Kim *et al*. [Appl. Phys. Lett. **78**, 3055 (2001)] and to evaluate higher-order azimuthal anchoring coefficients. Director behavior during switching is described in detail for general azimuthal directions of an applied electric field and the experimental results are explained on the basis of the theory. We obtain azimuthal anchoring coefficients up to the second higher-order term in an expansion of the anchoring energy function. Detailed analysis of the director behavior reveals a close analogy between the proposed model of nematic liquid crystal bistability and a coherent rotation (Stoner-Wohlfarth) model of ferromagnetism. This suggests a reversal-asymmetric property of the substrate-nematic interface director, differing from the reversal symmetry of the bulk nematic director, as far as the nematic bistability switching is concerned. © *2012 American Institute of Physics*. [http://dx.doi.org/10.1063/1.4716681]

I. INTRODUCTION

The bistability of liquid crystal (LC) directors, which appear in special cell configurations,[1–23] has long been one of the most important topics in the LC display industry. One of the main reasons for this is that bistable devices require no energy to maintain stable states, resulting in reduced power consumption. This characteristic has spurred the investigation and development of many kinds of display modes. In a series of studies,[10,20,22,23] we have been exploring nematic bistability on micropatterned alignment layer. Successful bistability switching has been demonstrated for alignment patterns fabricated using various methods including nanorubbing,[10] nanoimprint,[20] and photoalignment.[22,23] For practical applications, the photoalignment method is the best among them because of its high-throughput capability.[21] It was also shown that a pattern's geometric symmetry is unnecessary for bistability, which points to the possibility of using a novel maskless photoalignment method for fabricating large-area bistable patterns.[23]

Although the nanorubbing utilizing an atomic force microscope[10] and the photoalignment[22,23] are quite different in the experiment to fabricate bistable patterns composed of orthogonally aligned subdomains, we think that a bistability switching mechanism for these patterns is the same. In the original report, Kim *et al*.[10] proposed a switching mechanism of the nematic bistability based on a theoretical analysis. They showed that a π rotation of substrate-nematic interface director ($\boldsymbol{n}_0$) on a patterned layer is necessary to the bistability switching. They used the theory and measured switching field strength (E_{sw}) to obtain a reasonable value for a local azimuthal anchoring energy coefficient of the micropatterned layer. However, all the previous investigations,[10,20,22,23] including the original one, have been limited to one special case in which the azimuth of in-plane applied electric field (ϕ_E) was fixed and the anchoring function was assumed to be $(W_2/2)\sin^2\phi$ (Rapini-Papoular function), where W_2 is a anchoring coefficient and ϕ is an azimuth of $\boldsymbol{n}_0$ deflected from the alignment direction. This restriction has prevented us from verifying the proposed theory for more general ϕ_E and anchoring functions.

In this study, we investigate the azimuthal dependence of the switching field strength for a microchecker alignment layer to examine the validity of the proposed theory and also to evaluate higher-order azimuthal anchoring coefficients in an expansion of anchoring energy function. Our experimental results also supply information about a minimum value of E_{sw}, which in the past has been found to be very high.[10,20,22]

The rest of this paper is organized as follows. First, the switching behavior of the interface director is described in detail for general ϕ_E on the basis of the proposed switching mechanism. Next, we analyze and discuss the azimuthal dependence of the switching field strength. Finally, we point out a correspondence between the proposed theory of nematic bistability and a widely known model of ferromagnetic bistability, which provides us with a fresh view of the bistable system. We also discovered that the interface director behaves like a reversal-asymmetric vector, differing from the reversal symmetry of the bulk nematic director, as far as the switching of nematic bistability on micropatterned alignment layers is concerned.

[a)]Electronic mail: niitsuma@jaist.ac.jp.

II. EXPERIMENTAL

The alignment material we used was a photoalignable polyamic acid with azobenzene units.[24] A 1 wt. % solution of the polymer dissolved in *N*-methyl-2-pyrrolidone was spin-coated over a glass substrate ($50 \times 50 \times 0.7$ mm^3) and then soft-baked at 70 °C for 30 min on a hot plate. It was exposed to ultraviolet light (Ushio USH-250D lamp) passing through optical filters (Asahi Spectra LU0350 and SU0425) and a linear polarizer (CODIXX colorPol UV375 BC5 C355) first uniformly for 10 min and then with a microchecker photomask for 10 min. The linearly polarized ultraviolet (LPUV) light irradiation at normal incidence to the layer induced *trans-cis* isomerization, and successive thermal *cis-trans* relaxation of the azo group generated planar LC alignment without tilt angles. For the second exposure, the direction of polarization was perpendicular to that of the first exposure. Because of the reversibility of the isomerization, this process rotated (rewrote) the alignment direction in the illuminated region by π radians, creating a checker pattern in which the neighboring square subdomain units ($2.5 \times 2.5\ \mu$m^2) had orthogonal alignment directions. The LPUV doses were set so that the macroscopic stable orientation of the micropatterned alignment cell was $\pi/4$ from the orthogonal local alignment directions.

The absorption spectrum of the soft-baked alignment film on a quartz substrate and the irradiance spectrum of the LPUV light are shown in Fig. 1. UV spectrum peaks corresponded to the absorption band of the alignment polymer around 400 nm, which is responsible for the photoisomerization. The integrated irradiance of the UV light for $\lambda = 350$–425 nm was 6.2 mW/cm^2.

During the second exposure, the photomask and the substrate were in hard contact to avoid any diffraction effect. The hard-contact mode was performed using a silicone rubber sheet having 0.5 mm thickness and the same area as the photomask plate. The substrate was placed between the mask and the rubber sheet, which were in direct contact with each other around the substrate. One end of a silicone rubber tube reached the substrate through the rubber sheet and the other end was connected to a vacuum pump. The crossing part of the tube and the sheet was sealed with commercial silicone rubber sealant. In this apparatus, hard contact was achieved after a few seconds of pumping. The contact gap between the alignment layer substrate and the photomask was estimated from the interference color at < 100 nm, which was sufficiently small for micropatterning. Silicone rubber is suitable for hard contact due to its flexibility, adhesive property, and high resistance to UV and ozone exposures.

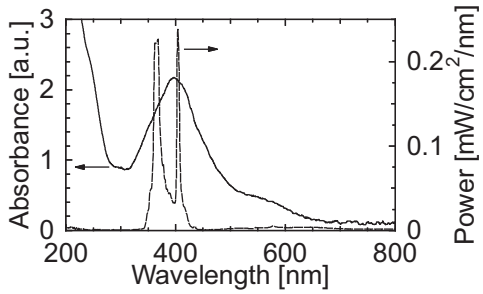

FIG. 1. Absorption spectrum of a soft-baked polymeric acid azo alignment film (solid curve) and irradiance spectrum of LPUV light (dashed curve). The integrated irradiance of UV light ($\lambda = 350$–425 nm) is 6.2 mW/cm^2.

The counter substrate with a uniform alignment orientation was prepared by using a similar photoalignment process. To build a bistable cell, the uniform alignment direction of the counter substrate was set to be parallel to one of the macroscopic stable orientations of the micropatterned substrate. The resulting nematic bistable states of the cell were homogeneous planar (H) and $\pi/2$-twisted planar (T) states, as shown in Figs. 2(a)–2(c). The T state was further divided into two states, left- and right-handed T states (LT and RT), in accordance with the twist sense.

The counter (top) substrate and the patterned (bottom) substrate were separated by 9 -μm-thick pieces of polyethylene naphthalate film (Teijin DuPont Films) and fixed with epoxy glue (Huntsman Araldite). The actual cell gaps (11 μm) were measured by interference spectroscopy. After injecting nematic LC 4-cyano-4′-pentylbiphenyl (5CB) at 50 °C in the isotropic phase, the cell was cooled to room temperature. The spin-coating, hard-contact process, and LC injection were all performed in clean air.

The electric field for switching was generated by quadrupole electrodes of indium tin oxide (ITO) on the bottom substrate. The field azimuth was controlled by changing the amplitude ratio of two in-phase synchronized sinusoidal voltage waves applied to the two orthogonal pairs of opposing electrodes [Fig. 2(d)]. The strength of the electric field component was defined as the root mean square of the applied voltage divided by the separation (300 μm) between the opposing electrodes. Voltage waves of 1 kHz frequency were generated by two synchronized function generators (Agilent 33220 A) followed by amplifiers (Matsusada HEOPT-3B20). The state of the cell in the region surrounded by the quadrupole electrodes was observed with an optical microscope

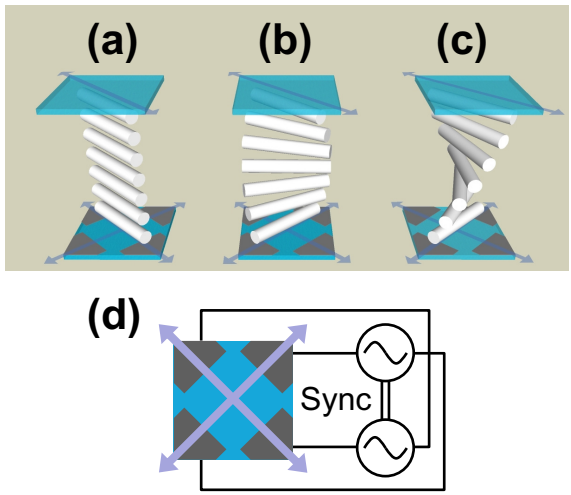

FIG. 2. Schematic of stable states and structure of nematic bistable cell. (a) Homogeneous planar (H) state. (b) Left- and (c) right-handed $\pi/2$-twisted (denoted as LT and RT, respectively) planar states. Rods indicate bulk directors. Stable alignment directions for LC on substrates are indicated by double-headed arrows. Quadrupole electrodes are also shown on the bottom substrate. (d) Connection between the synchronized voltage sources and the electrodes to generate azimuthally varying electric fields.

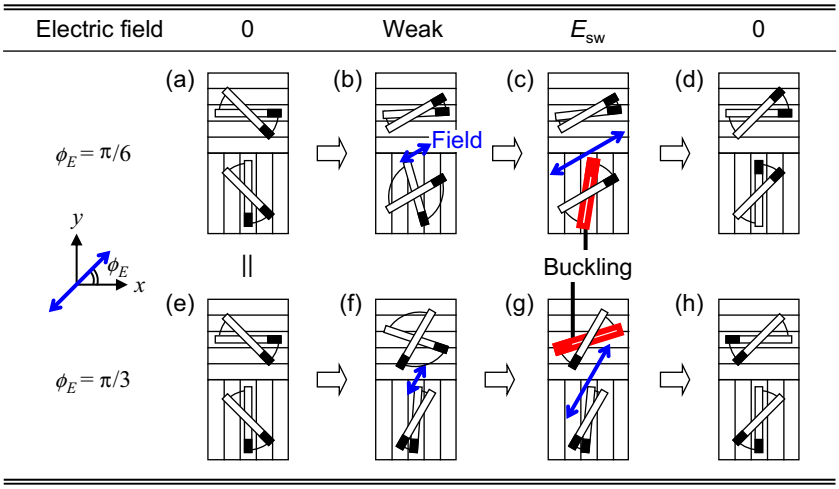

FIG. 3. Schematic top view of an interface director and a bulk director in H → T switching. Field azimuthal directions are $\pi/6$ for (a)–(d) and $\pi/3$ for (e)–(h). Square pair stands for the neighboring two subdomains with orthogonal local alignment directions depicted by stripes. Two superposed bars in each subdomain represent interface director (lower bar) and bulk director (upper bar). The black part of the bar indicates director's orientation. Twist angle between them is indicated by an arc. (a) and (e) Initial H state, (b) and (f) large twist appears in a weak field, (c) and (g) buckling occurs in a critical field, and (d) and (h) final LT and RT states, respectively. The counter substrate with an alignment direction of $-\pi/4$ is omitted for clarity.

(Olympus BX51) through crossed polarizers in UV-free illumination at room temperature.

III. DIRECTOR BEHAVIOR IN BISTABILITY SWITCHING

The director behavior in the switching from H state to T state is explained on the basis of the proposed switching mechanism[10] for two representative field azimuths. In Fig. 3, a two-square pair stands for the neighboring two types of subdomains that have orthogonal local alignment directions (x and y) depicted by stripes. The two superposed bars represent substrate-nematic interface director ($\boldsymbol{n}_0$, lower bar) and bulk director ($\boldsymbol{n}_b$, upper bar), which are parallel to the interface plane (the x-y plane). The director orientation is defined as the direction indicated by the black part of the bar. Although usually $\boldsymbol{n} = -\boldsymbol{n}$, we consider here a general case, $\boldsymbol{n} \neq -\boldsymbol{n}$, the reason for which will be clarified in the discussion. The alignment direction of the counter substrate is $-\pi/4$, which has been omitted from the figure for the sake of clarity.

Next, we describe the H → T switching process in detail. Figure 3(a) shows an initial field-off H state in which $\boldsymbol{n}_b$ makes a twist angle of $\pi/4$ with respect to $\boldsymbol{n}_0$. When a weak field with the direction $<\pi/4$, e.g., $\pi/6$, is applied to the cell, $\boldsymbol{n}_b$ homogeneously starts to rotate counterclockwise toward $\pi/6$ [Fig. 3(b)]. The orientation of $\boldsymbol{n}_0$ also deflects away counterclockwise from the alignment direction of each subdomain. At this stage, the x-aligned subdomain is in a stable state with a twist angle of $\sim\pi/6$ while the y-aligned subdomain is locally in a metastable state with a twist angle of $\sim 2\pi/3$. A local stable state of the y subdomain, in which $\boldsymbol{n}_b$ turns clockwise toward $-5\pi/6$ to make the twist angle smaller ($\sim\pi/3$), will not occur because it would require an in-plane π rotation (π wall) across the boundary between the x and y subdomains. Moreover, $\boldsymbol{n}_b$ cannot rotate clockwise toward $-5\pi/6$ homogeneously because its elastic free energy is higher than that of the uniform rotation toward $\pi/6$.

When the electric field strength increases to E_{sw}, the metastable state of the y subdomain is changed to a stable smaller-twist state by $\sim\pi$ rotation or buckling of $\boldsymbol{n}_0$ [Fig. 3(c)]. In this case, we say that the y subdomain is a switching subdomain. After the field is removed, $\boldsymbol{n}_b$ settles on the nearest macroscopic stable direction, $+\pi/4$, which leads to a LT state in combination with the director of the top counter substrate of $-\pi/4$ [Fig. 3(d)]. For different field directions $>\pi/4$, the switching occurs on the x subdomain and a RT state results, as shown in Figs. 3(e)–3(h). In the following section, we restrict our discussion to the H → T switching.

IV. RESULTS AND DISCUSSION

A. Azimuthal dependence of switching field strength

Figures 4(a) and 4(b) show optical micrographs of a H/T boundary region of the nematic bistability cell with different polarizer configurations. The cell orientation is the same as that shown in Fig. 3. The left half (bright) and right half (dark) of Fig. 4(a) are the T and H states, respectively. Two types of subdomain and a H/T boundary are clearly observed in Fig. 4(b). The bright (dark) square corresponds to the x (y) subdomain that was created by the first (second) LPUV exposure. The director at the boundary points to $\pi/2$. Figure 4(c) shows a large-area view of a H → T transitional state after an electric field was applied in the direction of $\phi_E = 10°$. In this field, H → LT switching occurred in a similar way to that shown in Figs. 3(a)–3(d). In the same figure, however, a RT state is also observed together with a reverse twist. This is due to inhomogeneous electric fields with $\phi_E > \pi/4$ near the electrodes, parts of which are seen as triangles at the corners of the image.

Figure 5(a) shows the dependence of the switching field strength for H → T transition on the azimuthal direction of the applied field. It should be noted that for $0 < \phi_E < \pi/4$, the switching occurs in the y subdomain and for $\pi/4 < \phi_E < \pi/2$, in the x subdomain (Sec. III). The gap of E_{sw} at $\phi_E = \pi/4$ therefore indicates the different azimuthal anchoring energies of the two subdomains. The minimum E_{sw} was measured around $\pi/4$ for both subdomains, which means it is difficult to reduce E_{sw} by changing ϕ_E.

Next, we explain the observed trend of $E_{sw}(\phi_E)$ on the basis of the proposed theory.[10] As was explained in Sec. III, E_{sw} is governed by the behavior of $\boldsymbol{n}_0$ in the switching subdomain. For simplicity, we assume that the electric field is

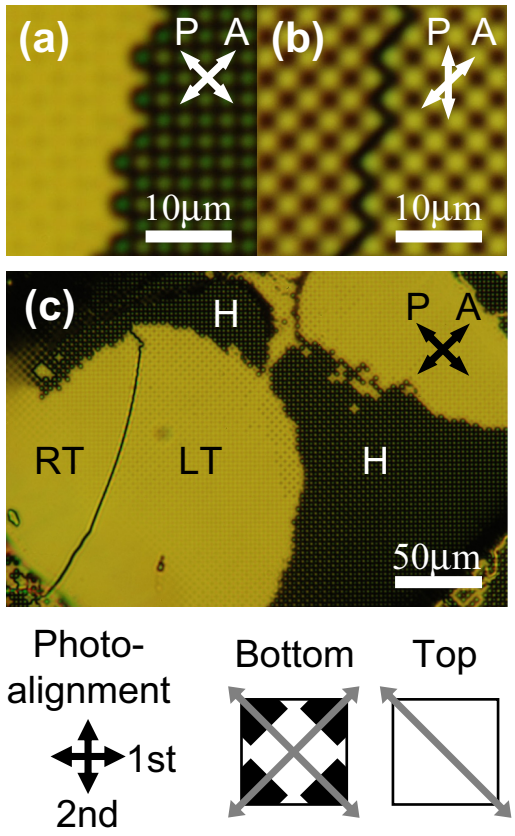

FIG. 4. (a) Optical micrograph of H/T boundary region. Left half (bright) and right half (dark) correspond to T and H states. (b) The same area observed with a different polarizer arrangement. Two types of square subdomain and H/T boundary are clearly seen. (c) Large-area view of a H → T transitional state after an electric field was applied in the $\phi_E = 10°$ direction. T state splits into LT and RT states with a reverse twist between them due to inhomogeneous electric field. Triangular areas at the corners show parts of quadrupole electrodes. The arrows labeled P and A indicate the polarizer and analyzer directions. Also shown are photoalignment directions caused by the first and second LPUV irradiations and the cell configuration.

uniform and parallel to the substrate through the cell, and the director is always planar accordingly. The free energy per unit area within the switching subdomain is expressed as[10]

$$F = \int_0^\infty \mathrm{d}z \left[\frac{1}{2}K_{22}(\phi'(z))^2 + \frac{1}{2}\varepsilon_0\Delta\varepsilon E^2\sin^2(\phi(z) - \phi_E)\right] + \sum_{n=1}^{\infty}\frac{W_{2n}}{2n}\sin^{2n}(\phi(0) - \alpha), \quad (1)$$

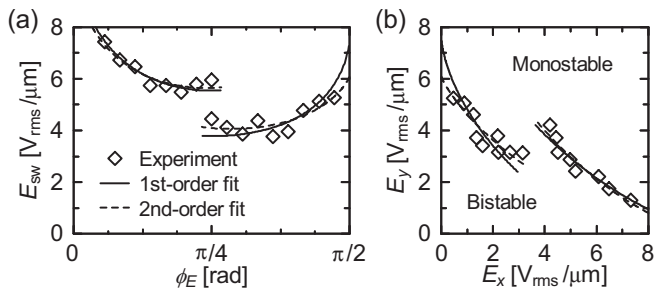

FIG. 5. (a) Azimuthal dependence of H → T switching field strength for $10° < \phi_E < 85°$. Solid and dashed curves are the best fits for the experimental data when anchoring energy functions are of first-order (only W_2 is non-zero) and of second-order (W_2 and W_4 are non-zero), respectively. (b) Polar plot of (a).

where K_{22} is a twist constant of LC (2×10^{-12} N for 5CB, Ref. 25), $\phi(z)$ is an azimuth of $\boldsymbol{n}_b$ at a vertical distance z from the substrate-nematic interface, $\varepsilon_0\Delta\varepsilon$ is a dielectric anisotropy of LC (7.2×10^{-11} F/m for 5CB, Ref. 26), W_{2n} is an azimuthal anchoring coefficient, and α is an alignment orientation angle of the x or y subdomain (0 or $\pi/2$). We also assumed here an infinitely thick cell. The first term is the sum of LC elastic free energy and interaction energy between LC and in-plane electric field. The second term represents a generalized azimuthal anchoring energy function. The Euler-Lagrange procedure and integration of the result in z give $\phi'(z) = -E\sqrt{\varepsilon_0\Delta\varepsilon/K_{22}}\,\sin(\phi - \phi_E)$ under strain-free and no-anchoring conditions at infinity: $\phi'(\infty) = 0$ and $\phi(\infty) = \phi_E$. Inserting this into Eq. (1) and changing the integration variable from z to ϕ yield the following expression for a free energy (with a dropped constant term):

$$f(\phi_0) = F/W_2 = -q\cos(\phi_0 - \phi_E) + \sum_{n=1}^{\infty} w_{2n}\sin^{2n}(\phi_0 - \alpha),$$

where $\phi_0 = \phi(0)$, $q = \sqrt{\varepsilon_0\Delta\varepsilon K_{22}}E/W_2$, and $w_{2n} = W_{2n}/2nW_2$. The first term, which is rewritten as $-q\boldsymbol{n}_0\cdot\boldsymbol{E}$, can be considered an interaction between the interface director and the electric field, with the bulk effects being included in q. The large twist before buckling [Figs. 3(b) and 3(f)] can be described using this term. The stable equilibrium azimuth angles of $\boldsymbol{n}_0$ are obtained from $\partial f/\partial\phi_0 = 0$ and $\partial^2 f/\partial\phi_0^2 > 0$, which determine the local minima of the free energy. The buckling of $\boldsymbol{n}_0$ occurs when the field increases to E_{sw} at which the second derivative becomes zero and then one of the minima disappears. For example, when $w_{2n} = 0$ for $n \geq 2$, we obtain

$$E_{sw}(\phi_E) = \frac{W_2}{\sqrt{\varepsilon_0\Delta\varepsilon K_{22}}}f(\phi_E);$$
$$f(\phi_E) = (\sin^{2/3}\phi_E + \cos^{2/3}\phi_E)^{-3/2}. \quad (2)$$

The equivalence to a more complex expression,[27]

$$f(\phi_E) = \sqrt{1 + 3\cos^2[2\arctan(\tan^{1/3}\phi_E)]}/2$$

is straightforward through trigonometric identities including $\arctan x = \arccos(1/\sqrt{1+x^2})$ and some algebraic operations.

The solid curves shown in Fig. 5(a) are the best fits for the data using Eq. (2). They take a minimum at $\pi/4$ and account for the observed tendency of $E_{sw}(\phi_E)$, confirming the validity of the proposed theory. The fitting parameters yielded the anchoring coefficients $W_2 = 8.9 \times 10^{-5}$ J/m^2 and 1.3×10^{-4} J/m^2 for the x and y subdomains, respectively. The dashed curves in the same figure are the fit results by using an anchoring energy function with non-zero W_2 and W_4. In this case, the expression of E_{sw} is not as simple as Eq. (2). As a result, we obtained a better fit for the x subdomain with $W_2 = 1.2 \times 10^{-4}$ J/m^2 and $W_4 = -4.5 \times 10^{-5}$ J/m^2 whereas for the y subdomain, W_4 was negligibly small compared to the experimental error.

We should note here that the photoalignment conditions were different for the two subdomains. The y subdomain was created by rewriting a LPUV-treated film in which alignment polymers were well-oriented, and therefore, a higher rate of photoisomerization, or a larger W_2, could be expected than in the x subdomain, which was generated from a non-treated film in which alignment polymers were randomly oriented. This suggests that the difference in the azimuthal anchoring properties, which reflect the order parameter of the alignment molecules, between the two subdomains might be caused by different initial molecular orientations in the photoalignment film. The finite negative W_4 observed in the x subdomain might also be an effect of the lower order parameter of the alignment molecules.

B. Analogy with coherent rotation (CR) model

Here, we discuss an analogy between the nematic bistability system and CR or Stoner-Wohlfarth model[28,29] in ferromagnetism, a typical bistable system. The CR model describes the behavior of the magnetization vector of a single-domain particle in a magnetic field under an anisotropic constraint (demagnetizing energy and shape anisotropy energy) in a two-dimensional space. This analogy will be easier to understand if we observe the correspondence between the physical quantities appearing in the two systems (see Table I). We can say, for example, that the buckling of $\boldsymbol{n}_0$ in an electric field is a counterpart of a Barkhausen jump (a sudden reversal of magnetization vector) in a magnetic field.

One may wonder why a director and a magnetization vector can be treated on an equal basis since they have different properties: typically a director will have reversal symmetry ($\boldsymbol{n}=-\boldsymbol{n}$) and a fixed norm ($|\boldsymbol{n}|=1$) whereas a magnetization vector, $\boldsymbol{m}$, has no such restrictions. The answer is that $\boldsymbol{n}_0$ has to be considered a reversal-asymmetric vector ($\boldsymbol{n}_0 \neq -\boldsymbol{n}_0$) as far as the switching of the nematic bistability is concerned and $|\boldsymbol{m}|$ is assumed to be fixed in the CR model. The apparent asymmetric nature of $\boldsymbol{n}_0$ manifests itself in the large-angle twisting and successive buckling of $\boldsymbol{n}_0$ in switching (Sec. III). This means that we need to distinguish $\boldsymbol{n}_0$ and $-\boldsymbol{n}_0$ in a switching subdomain because they correspond to different bistable bulk states one-to-one.

We now apply CR theory to analyzing the nematic bistability on micropatterned alignment layers. One of the typical results derived from the theory is that E_{sw} forms a characteristic curve in a polar plot, which is of great use in graphically representing stability properties.[29,30] For example, we can rewrite Eq. (2) as

$$E_{\mathrm{sw},x}^{2/3}+E_{\mathrm{sw},y}^{2/3}=E_{\mathrm{sw}}^{2/3}(0),$$

where $E_x=E\cos\phi_E$ and $E_y=E\sin\phi_E$. This is an equation of an astroid in the E_x-E_y plane. In a general case, i.e., $w_{2n}\neq 0$ for any n, there exists a different characteristic curve parameterized by ϕ_0. Figure 5(b) shows a polar plot of Fig. 5(a). The quadrant is divided into two regions by the critical curve, and the system is bistable inside the curve and monostable outside. The switching process can be considered a transfer of one of the bistable states to the other through a monostable state that is realized in a strong external field $>E_{\mathrm{sw}}(\phi_E)$. One can readily evaluate the azimuthal dependence of switching field strength for different values of W_{2n} in a like manner. This procedure has potential use in the design of anchoring properties for devices with improved nematic bistability.

TABLE I. Corresponding physical quantities appearing in the nematic LC bistability and coherent rotation model in ferromagnetism.

	LC bistability	Coherent rotation model
Rotating vector	Interface director	Magnetization vector
External field	Electric field	Magnetic field
Anisotropic constraint	Anchoring energy	Anisotropic energy

V. SUMMARY

In this study, we investigated the azimuthal dependence of the switching field strength of nematic bistability on micropatterned alignment layers to determine the validity of the proposed switching theory and to evaluate higher-order azimuthal anchoring coefficients of the alignment layer. Detailed behavior of directors in H → T switching was analyzed for the general azimuthal direction of an applied field, with results showing that the switching subdomain interchanged at a critical field angle of $\pi/4$. This means that the azimuthal anchoring energy of each subdomain can be estimated by measuring the switching field strength for azimuthal directions from, e.g., 0 to $\pi/2$. The agreement between the theory and the experimental data demonstrated the validity of the proposed theory as well as the difficulty in reducing E_{sw} by changing ϕ_E. We obtained anchoring coefficients for the two subdomains separately up to the second higher-order term in an expansion of the azimuthal anchoring energy function by fitting. The difference in anchoring coefficients for the two subdomains suggests an influence of the initial state of photoalignment film on its anchoring properties.

The analogy between the proposed model of nematic LC bistability and the coherent rotation model of ferromagnetism suggested that the interface director behaves like a reversal-asymmetric vector as far as the nematic bistability switching is concerned. In fact, the asymmetric nature can be seen in the large-angle twisting and successive buckling of the interface director in the switching subdomain. The critical curve of the switching field may be helpful for investigating the nematic bistability on micropatterned alignment layers for a general azimuthal anchoring energy function.

ACKNOWLEDGMENT

J.N. thanks Dr. Y. Mitsuhashi for his continuous encouragement.

[1] G. D. Boyd, J. Cheng, and P. D. T. Ngo, Appl. Phys. Lett. **36**, 556 (1980).
[2] D. W. Berreman and W. R. Heffner, J. Appl. Phys. **52**, 3032 (1981).
[3] H. L. Ong, R. B. Meyer, and A. J. Hurd, J. Appl. Phys. **55**, 2809 (1984).
[4] R. Barberi, M. Baix, and G. Durand, Appl. Phys. Lett. **55**, 2506 (1989).
[5] S. P. Palto, S. G. Yudin, C. Germain, and G. Durand, J. Phys. II **5**, 133 (1995).
[6] I. Dozov, M. Nobili, and G. Durand, Appl. Phys. Lett. **70**, 1179 (1997).

[7]R. Barberi, J. J. Bonvent, M. Giocondo, M. Iovane, and A. L. Alexe-Ionescu, J. Appl. Phys. **84**, 1321 (1998).
[8]Z. L. Xie and H. S. Kwok, J. Appl. Phys. **84**, 77 (1998).
[9]J.-X. Guo, Z.-G. Meng, M. Wong, and H.-S. Kwok, Appl. Phys. Lett. **77**, 3716 (2000).
[10]J.-H. Kim, M. Yoneya, J. Yamamoto, and H. Yokoyama, Appl. Phys. Lett. **78**, 3055 (2001).
[11]C. Joubert, J. Angele, A. Boissier, P. Dave, I. Dozov, T. Elbhar, B. Pecout, D. Stoenescu, R. Vercelleto, and P. Martinot-Lagarde, SID Symp. Digest Tech. Papers **33**, 30 (2002).
[12]M. Stalder and M. Schadt, Liq. Cryst. **30**, 285 (2003).
[13]F. S. Y. Yeung and H. S. Kwok, Appl. Phys. Lett. **83**, 4291 (2003).
[14]D. D. Huang, E. P. Pozhidaev, V. G. Chigrinov, H. L. Cheung, Y. L. Ho, and H. S. Kwok, Displays **25**, 21 (2004).
[15]I. M. Syed, G. Carbone, C. Rosenblatt, and B. Wen, J. Appl. Phys. **98**, 034303 (2005).
[16]E. Pozhidaev, V. Chigrinov, and X. Li, Jpn. J. Appl. Phys., Part 1 **45**, 875 (2006).
[17]T.-H. Lin, H.-C. Jau, S.-Y. Hung, H.-R. Fuh, and A. Y.-G. Fuh, Appl. Phys. Lett. **89**, 021116 (2006).
[18]E.-K. Lee and J.-H. Kim, J. Appl. Phys. **102**, 036102 (2007).
[19]C. Tsakonas, A. J. Davidson, C. V. Brown, and N. J. Mottram, Appl. Phys. Lett. **90**, 111913 (2007).
[20]J. S. Gwag, J. Fukuda, M. Yoneya, and H. Yokoyama, Appl. Phys. Lett. **91**, 073504 (2007).
[21]V. G. Chigrinov, V. M. Kozenkov, and H.-S. Kwok, *Photoalignment of Liquid Crystalline Materials: Physics and Applications* (Wiley, Chichester, 2008).
[22]J. Niitsuma, M. Yoneya, and H. Yokoyama, Appl. Phys. Lett. **92**, 241120 (2008).
[23]J. Niitsuma, M. Yoneya, and H. Yokoyama, Liq. Cryst. **37**, 31 (2010).
[24]B. Park, Y. Jung, H.-H. Choi, H.-K. Hwang, Y. Kim, S. Lee, S.-H. Jang, M. Kakimoto, and H. Takezoe, Jpn. J. Appl. Phys., Part 1 **37**, 5663 (1998).
[25]N. V. Madhusudana and R. Pratibah, Mol. Cryst. Liq. Cryst. **89**, 249 (1982).
[26]H. Yokoyama and H. A. van Sprang, J. Appl. Phys. **57**, 4520 (1985).
[27]J.-H. Kim, M. Yoneya, and H. Yokoyama, Nature **420**, 159 (2002).
[28]E. C. Stoner and E. P. Wohlfarth, Philos. Trans. R. Soc. London, Ser. A **240**, 599 (1948). Reprinted in IEEE Trans. Magn. **27**, 3475 (1991).
[29]G. Bertotti, *Hysteresis in Magnetism* (Academic, San Diego, 1998), chap. 8.
[30]A. Thiaville, J. Magn. Magn. Mater. **182**, 5 (1998).